PAPER

CrossMark
click for updates

Novel efficient hole-transporting materials based on a 1,1′-bi-2-naphthol core for perovskite solar cells†

Wenhua Qiao, Yu Chen,* Fusheng Li, Xueping Zong, Zhe Sun, Mao Liang and Song Xue*

New star-shaped and efficient hole-transporting materials based on a 1,1′-bi-2-naphthol central core for perovskite solar cells are developed *via* facile synthesis. The 1,1′-bi-2-naphthol is first applied into the field of perovskite solar cells. The 2,7-carbazole-bis(4-methoxy-phenyl)-amine and 3,6-carbazole-bis(4-methoxy-phenyl)-amine are used as end groups. A reference compound based on a 3,3′-biphenyl core is prepared as well. The new materials have suitable highest occupied molecular orbital levels to match well with the valence band of $CH_3NH_3PbI_3$, and they all exhibit a glass transition temperature higher than 160 °C. A device fabricated by hole-transporting materials based on 1,1′-bi-2-naphthol and 2,7-carbazole-bis(4-methoxy-phenyl)-amine in conjunction with a carbon counter electrode achieves the highest power conversion efficiency of 8.38% under the illumination of 100 mW cm^{-2}, which is comparable to that fabricated by commercial spiro-OMeTAD (8.73%). Dark current, IPCE and IMVS measurements are also discussed. The introduction of 2,7-carbazole-bis(4-methoxy-phenyl)-amine onto the 1,1′-bi-2-naphthol central core tends to enhance J_{sc} of a device, and 3,6-carbazole-bis(4-methoxy-phenyl)-amine improves V_{oc}. This work provides a new series of hole-transporting materials to fabricate economic and efficient perovskite solar cells.

1. Introduction

Hybrid organic–inorganic perovskite solar cell (PSC) systems have achieved high efficiency up to 20%.[1–5] Researchers have been intrigued to explore more possibilities for finding new efficient materials and better understanding interfacial mechanisms.[6–10] The solid-state hole-transporting materials (HTMs) have been introduced into PSC construction, effectively enhancing the power conversion efficiency (PCE). The state-of-the-art HTM is an organic small molecule based on the spirobifluorene core,[11,12] 2,2′,7,7′-tetrakis-(N,N-di-p-methoxyphenylamine)-9,9′-spirobifluorene (spiro-OMeTAD). Alternative comparable organic small-molecule HTMs also have been developed for fabricating PSC,[13–16] due to facial synthesis, low cost and easy to structural modification. The advantage of organic small-molecule HTMs is the property of HTM solution can realize good infiltration into perovskite layer and flexible tuning energy level to match the energy band of organolead halide perovskite and counter electrode.[17,18] The reported structure of organic small-molecule HTMs for PSC mainly includes linear and star shapes.[19–22] The commonly used donor groups of organic small-molecule HTMs are derivatives of diphenylamine and triphenylamine, and the newly emerged carbazole–diphenylamines facilitating the HTM with fast charge-transport property.

Several new star-shaped HTMs based on bridged/spiro central core were found to be similarly efficient as spiro-OMeTAD. The structure of central core has an impact on the thermal stability of the star-shaped HTM and the solid state of spin-coated HTM film.[23,24] The commercial spiro-OMeTAD shows a glass transition temperature (T_g) of 125 °C.[25] According to reports, a HTM based on a swivel-cruciform 3,3′-bithiophene core in PSC showed an amorphous state and a comparable PCE of 11.0% ($T_g = 65$ °C) to that derived from spiro-OMeTAD (11.4%);[26] a HTM based on a spiro-bipropylenedioxythiophene core tends to crystallize in the solid state, and its photovoltaic performance in PSC (the highest PCE is 13.44%, $T_g = 175$ °C) was as good as device obtained using spiro-OMeTAD (12.16%) under the same conditions;[27] a HTM based on a [2,2]paracyclophane core in PSC yielded a PCE of 17.6% ($T_g = 148.5$ °C), and the spiro-OMeTAD HTM displayed a 15.4% in the same situation.[28] The bridged/spiro core structures of HTM provide a three-dimensional (3D) skeleton, and it is reported the 3D structure of the star-shaped HTM favors the property of charge transport.[29–31] These findings offer

Tianjin Key Laboratory of Organic Solar Cells and Photochemical Conversion, School of Chemistry & Chemical Engineering, Tianjin University of Technology, Tianjin 300384, P. R. China. E-mail: cy26tj@icloud.com; xuesong@ustc.edu.cn; Fax: +86-22-60214252

inspiration to the development of the bridged/spiro core based HTMs that used for constructing economical and highly efficient PSCs.

Recently, we have synthesized star-shaped HTMs based on 1,1′-bi-2-naphthol (BINOL) core, and it displays a good performance in PSC. Note that, the BINOL-based HTMs show greater advantage over our previously reported HTMs.[32,33] To our best knowledge, it is the first time for BINOL compounds to be reported in PSC field. BINOL is a typical C2-symmetric aromatic compounds,[34,35] and it is often used as a ligand for transition-metal catalyzed asymmetric synthesis,[36–40] a donor group for charge-transfer complex applied in molecular recognition,[41–43] and a structural skeleton for fluorescent chemical sensors for enantioselective fluorescent recognition.[44,45] BINOL is a commercial and low-cost compound, and its C2-symmetric feature is good for developing star-shaped HTM with 3D structure. In this work, two HTMs based on a BINOL core and carbazole–diphenylamine arms were studied. The hydroxyl groups of the BINOL were replaced by methoxyl group via etherification reaction.[43]

In this paper, we report the synthesis and characterization of two new HTMs based on a BINOL central core, 9,9′-(2,2′-dimethoxy-1,1′binaphthyl-6,6′-diyl)bis(N^2,N^2, N^7,N^7-tetrakis(4-methoxy-phenyl)-9H-carbazole-2,7-diamine) (Q197) and 9,9′-(2,2′-dimethoxy-1,1′binaphthyl-6,6′-diyl)bis(N^3,N^3,N^6,N^6-tetrakis (4-methoxy-phenyl)-9H-carbazole-3,6-diamine) (Q205). A reference HTM based on a 3,3′-biphenyl central core, 9,9′-(6,6′-dimethoxy-biphenyl-3,3′-diyl)bis(N^2,N^2,N^7,N^7-tetrakis (4-methoxy-phenyl)-9H-carbazole-2,7-diamine) (Q198), was prepared for a comparative study. The structures of Q197, Q198, and Q205 are shown in Fig. 1. The donor groups for the three HTMs are carbazole-bis(4-methoxy-phenyl)-amine. The bis(4-methoxy-phenyl)-amine moiety is replaced on different positions of 9H-carbazole. The donor group of Q197 and Q198 is 2,7-carbazole-bis(4-methoxy-phenyl)-amine, and that of Q205 is 3,6-carbazole-bis(4-methoxy-phenyl)-amine. The spectra of the studied HTMs were investigated for their absorption ability in solution and on the perovskite film. The electrochemical measurements and theoretical calculations were conducted for determining energy levels and optimizing geometric structures of the HTMs. Their thermal stability was evaluated by differential scanning calorimetry (DSC) and thermogravimetry (TG). PSCs based on the BINOL-based HTMs were fabricated, and the corresponding photovoltaic performances were compared with that of device fabricated by the reference HTM. The results indicate that the HTM based on the BINOL central core has a great potential for constructing high-efficiency PSC.

2. Experimental

2.1. Instrument and materials

All reactions were carried out under argon conditions and solvents were distilled from analytical grade reagents. The BINOL, Pd₂(dba)₃, n-butyllithium, t-BuONa, (t-Bu)₃P were
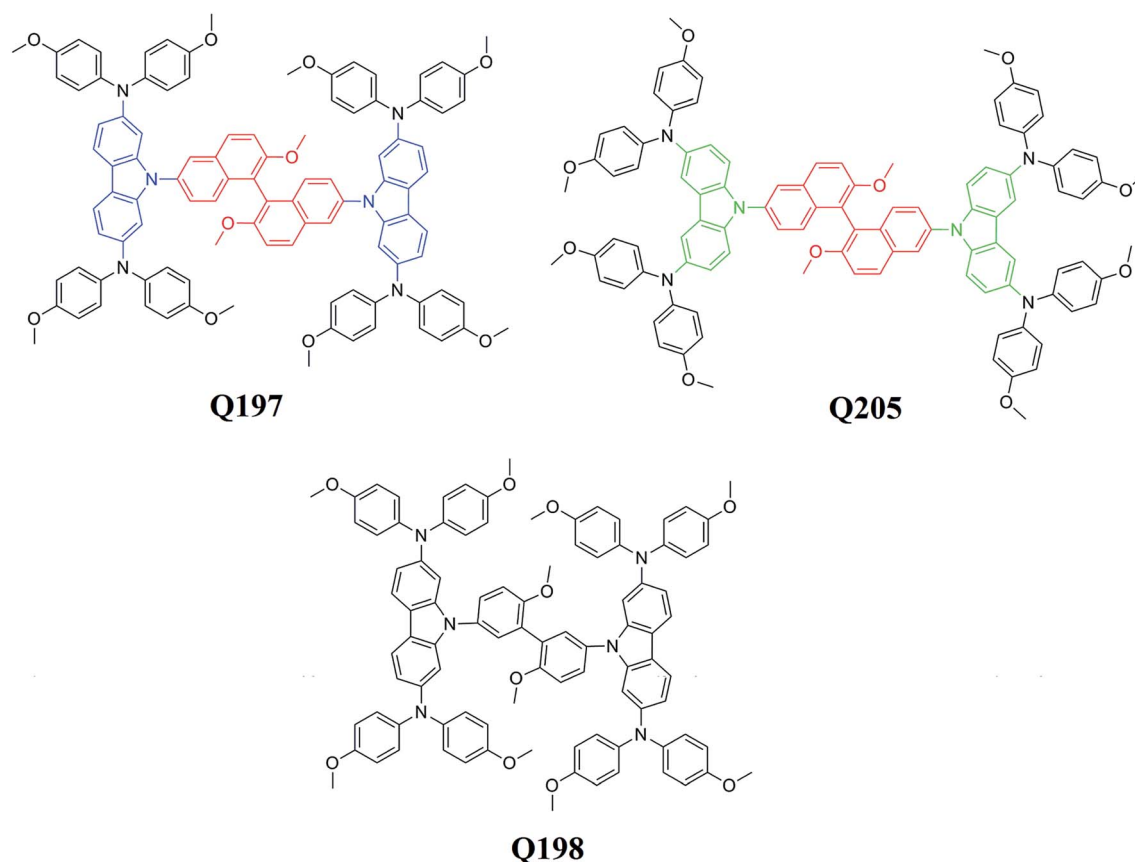

Fig. 1 Structures of Q205, Q197 and Q198.

purchased from Energy Chemical (China). The lithium bis(tri-fluoromethanesulfonyl)imide (LiTFSI, 0.1 M) and 4-*tert*-pyridine (TBP) were purchased from Aldrich. The melting points of the samples were measured with a RY-1 melting point apparatus (Tianfen, China), and temperatures were uncorrected. ^{1}H NMR and ^{13}C NMR spectra were recorded on a Bruker AM-400 spectrometer. The reported chemical shifts were referenced against TMS. High resolution mass spectra (HRMS) were obtained with a Micromass GCT-TOF mass spectrometer.

2.2. Synthesis

The synthesis route for **Q205**, **Q197** and **Q198** are shown in Scheme 1. Intermediates from compound **1**, **5**, **6** and **7** were known compounds, and they were prepared by following synthetic methods reported in the literatures.[46-50]

Synthesis of 9,9′-(2,2′-dimethoxy-1,1′binaphthyl-6,6′-diyl)-bis(N^3,N^3,N^6,N^6-tetrakis(4-methoxy-phenyl)-9H-carbazole-3,6-diamine) (Q205). The compound **Q205** was obtained by Buchwald–Hartwig reaction. Compound **1** (1 g, 1.69 mmol), compound **6** (0.20 g, 0.42 mmol) and *t*-BuONa (0.19 g, 8.73 mmol) was added to 20 mL of anhydrous toluene. The system was purged with nitrogen several times. Then (*t*-Bu)$_3$P (0.017 g, 12% mol) and Pd$_2$(bda)$_3$ (0.039 g, 6% mol) were placed in mixture solution and the reaction was refluxed for 24 h. After cooling to room temperature and 20 mL water was added. Organic phase separation by ethyl acetate (3 × 20 mL) and combined organic phases were dried with MgSO$_4$ and purified by column chromatography petroleum ether/ethyl acetate (PE/EtOAc = 2 : 1, R_f = 0.2) to afford 0.50 g of **Q205** with yield of 76% as green solids. Mp: 115–117 °C; ^{1}H NMR (400 MHz, DMSO-d_6), δ (ppm): 8.24 (4H, d, J = 7.3 Hz), 7.79–7.66 (6H, m), 7.49 (2H, d, J = 9.1 Hz), 7.34 (4H, d, J = 8.8 Hz), 7.24 (2H, d, J = 9.0 Hz), 7.05 (4H, d, J = 8.6 Hz), 6.86 (16H, d, J = 9.0 Hz), 6.80 (16H, d, J = 9.0 Hz), 3.81 (6H, s), 3.68 (24H, s). ^{13}C NMR (100 MHz, pyridine-d_5) δ 156.05, 155.11, 142.84, 142.08, 138.23, 133.38, 133.34, 130.13, 129.99, 127.44, 125.78, 125.40, 125.09, 124.52, 119.61, 117.40, 115.34, 114.95, 111.17, 56.34, 55.20. HRMS (ESI) (*m/z*): [M]$^+$ calcd for C$_{102}$H$_{84}$N$_6$O$_{10}$, 1553.6249; found: 1553.6327.

Synthesis of 9-benzyl-2,7-dibromo-9H-carbazole (2). NaH (0.55 g, 23.08 mmol) was added in one portion to anhydrous DMF (50 mL). A solution of 2,7-dibromo-9H-carbazole (5.00 g, 15.38 mmol) in DMF (20 mL) was added dropwise. After one hour, benzyl bromide (1.83 mL, 15.38 mmol) was added slowly. The suspension was stirred for another 6 h under nitrogen and carefully quenched with water. Then precipitate was filtrated to give white precipitate with quantitative yield, 6.38 g. ^{1}H NMR (400 MHz, DMSO-d_6), δ (ppm): δ 8.17 (2H, d, J = 8.32 Hz), 7.92 (2H, s), 7.39 (2H, d, J = 8.32 Hz), 7.31–7.22 (3H, m), 7.12 (2H, d, J = 7.16 Hz), 5.71 (2H, s).

Synthesis of 9-benzyl-N^2,N^2,N^7,N^7-tetrakis(4-methoxyphenyl)-9H-carbazole-2,7-diamine (3). Compound **2** (5.0 g, 12.04 mmol), 4,4′-dimethoxydiphenylamine (6.07 g, 26.5 mmol) and *t*-BuONa (2.88 g, 30.01 mmol) were put in the round bottom flask equipped with stirring bar in anhydrous toluene (60 mL). Then (*t*-Bu)$_3$P (0.38 g, 15% mol), and Pd$_2$(bda)$_3$ (0.74 g, 4% mol)

were added under nitrogen. The mixture was refluxed and the reaction was followed by TLC (thin layer chromatography). Reaction was completed after 24 hours. The aqueous phase was extracted with CH$_2$Cl$_2$ (3 × 50 mL). The combined organic phases were dried with MgSO$_4$ and purified by column chromatography (PE/EtOAc = 5 : 1) to afford 6.5 g (76% yield) of compound **3**. ^{1}H NMR (400 MHz, DMSO-d_6) δ 7.78 (2H, d, J = 8.44 Hz), 7.22 (2H, d, J = 2.24 Hz), 7.21 (1H, s), 6.95 (12H, d, J = 8.96 Hz), 6.86 (8H, d, J = 9 Hz), 6.66 (2H, dd, J = 1.76 Hz, J = 8.40 Hz), 5.18 (2H, s), 3.73 (12H, s).

Synthesis of N^2,N^2,N^7,N^7-tetrakis(4-methoxyphenyl)-9H-carbazole-2,7-diamine (4). To a stirred of compound **3** (2.90 g, 4.07 mmol) in 120 mL DMSO was added *t*-BuOK (40.74 mmol) at room temperature. The reaction mixture was stirred for 20 min and O$_2$ was bubbled for the reaction with 3 h. Then water (200 mL) was poured to reaction solution and the mixture was stirred overnight. The precipitate was filtrated and purified by column chromatography with petroleum ether/ethyl acetate (PE/EtOAc = 4 : 1) to give a light yellow solid compound **4** (2.1 g). Yield: 63%. ^{1}H NMR (400 MHz, DMSO-d_6), δ (ppm): 7.74 (2H, d, J = 8.44 Hz), 6.99 (8H, d, J = 9 Hz), 6.89 (8H, d, J = 9 Hz), 6.76 (2H, d, J = 1.84 Hz), 6.66 (2H, dd, J = 1.96 Hz, J = 8.44 Hz), 3.74 (12H, s).

Synthesis of 9,9′-(2,2′-dimethoxy-1,1′binaphthyl-6,6′-diyl)bis(N^2,N^2,N^7,N^7-tetrakis(4-methoxy-phenyl)-9H-carbazole-2,7-diamine) (Q197). Compound **4** (1 g, 1.69 mmol), compound **6** (0.20 g, 0.42 mmol) and *t*-BuONa (0.19 g, 8.73 mmol) were added to 20 mL of anhydrous toluene. The system was purged with nitrogen several times. Then (*t*-Bu)$_3$P (0.017 g, 12% mol) and Pd$_2$(bda)$_3$ (0.039 g, 6% mol) were added to the mixture solution and the reaction was refluxed for 24 h. The reaction was cooled to room temperature and 20 mL water was added. The mixture were extracted by ethyl acetate and the combined organic phases were dried with MgSO$_4$ and purified by column chromatography (petroleum ether/ethyl acetate = 2 : 1) to afford 0.50 g of **Q197** with yield of 76% as brown solids. Mp: 185–186 °C; ^{1}H NMR (400 MHz, DMSO-d_6), δ (ppm): δ 8.00 (2H, d, J = 8.48 Hz), 7.93 (2H, s), 7.77 (4H, d, J = 8.44 Hz), 7.64 (2H, d, J = 9.28 Hz), 7.17 (2H, d, J = 8.88 Hz), 7.00 (2H, d, J = 9.00 Hz), 6.92 (16H, d, J = 8.60 Hz), 6.86 (4H, s), 6.75 (16H, d, J = 8.56 Hz), 6.69 (4H, d, J = 9.20 Hz), 3.64 (6H, s), 3.59 (24H, s) ^{13}C NMR (100 MHz, DMSO-d_6) δ 155.70, 155.55, 146.81, 141.78, 141.14, 132.42, 132.21, 129.88, 129.31, 126.67, 126.32, 125.10, 124.42, 120.54, 118.70, 117.69, 115.57, 115.19, 101.76, 56.55, 55.57. HRMS (ESI) (*m/z*): [M]$^+$ calcd for C$_{102}$H$_{84}$N$_6$O$_{10}$, 1553.6249; found: 1553.6282.

Synthesis of 9,9′-(6,6′-dimethoxy-biphenyl-3,3′-diyl)bis(N^2,N^2,N^7,N^7-tetrakis(4-methoxy-phenyl)-9H-carbazole-2,7-diamine) (Q198). Compound **4** (1 g, 1.69 mmol), compound **7** (0.15 g, 0.42 mmol) and *t*-BuONa (0.19 g, 8.73 mmol) were added to 20 mL of anhydrous toluene. The system was purged with nitrogen several times. Then (*t*-Bu)$_3$P (0.017 g, 12% mol) and Pd$_2$(bda)$_3$ (0.039 g, 6% mol) were added to the mixture and the reaction was refluxed for 24 h. After cooling to room temperature 20 mL water was added to the reaction mixture. Organic phase separation by ethyl acetate (3 × 20 mL) and combined organic phases were dried with MgSO$_4$ and purified by column chromatography (petroleum ether/ethyl acetate = 2 : 1) to

afford 0.50 g **Q198** with yield of 64% as brown solids. Mp: 176–178 °C; ^{1}H NMR (400 MHz, DMSO-d_6), δ (ppm): 7.79 (4H, d, J = 8.40 Hz), 7.31 (2H, d, J = 8.20 Hz), 6.99 (3H, d, J = 8.80 Hz), 6.87 (19H, d, J = 8.12 Hz), 6.67–6.60 (22H, m), 3.62 (6H, s), 3.48 (24H, s). ^{13}C NMR (100 MHz, DMSO-d_6) δ 156.32, 155.85, 147.01, 142.52, 140.96, 129.31, 129.12, 128.95, 128.46, 127.76, 126.88, 120.56, 117.13, 115.20, 113.35, 56.23, 55.42. HRMS (ESI) (m/z): [M]$^+$ calcd for $C_{94}H_{85}N_6O_{10}$, 1457.6249; found: 1457.6327.

2.3. Spectral, electrochemical and thermal stability measurements

The absorption spectra of **Q205**, **Q197** and **Q198** in solution and coated on mesoporous TiO_2 and $TiO_2/CH_3NH_3PbI_3$ films were measured by SHIMADZU UV-2600 spectrophotometer. Fluorescence measurements were carried out with a HITACHI F-4500 fluorescence spectrophotometer. The morphology and structural properties of the films were analyzed using a ULTRA plus ZEISS field emission scanning electron microscope (SEM) and a Bruker AXS-D8 Advance X-ray diffractometer (XRD) using Cu Kα radiation.

Cyclic voltammetry (CV) measurements for **Q205**, **Q197** and **Q198** were performed on a Zennium electrochemical workstation (ZAHNER, Germany) using a three-electrode system. Tetrabutylammonium hexafluorophosphate (n-Bu$_4$NPF$_6$) of 0.1 M was added into a dichloromethane solution as electrolyte. An Ag/0.01 M AgNO$_3$ electrode (acetonitrile as solvent) was used as the reference electrode. In three-electrode system, a FTO conductive glass was used as the working electrode, and a platinized carbon electrode was used as the counter electrode. The scan rates were 10 mV s^{-1}. The measurements were calibrated using ferrocene as standard. The redox potential of ferrocene internal reference is taken as 0.63 V *versus* NHE.

The thermal stability was determined by thermogravimetry (TG) and differential scanning calorimetry (DSC). TG analyses were performed on TG 209 F3 Tarsus (NETZSCH, Germany) at a heating rate of 10 °C min^{-1} under nitrogen atmosphere. DSC analyses were conducted on DSC 200 F3 Maia (NETZSCH, Germany) at a heating rate of 10 °C min^{-1} under a nitrogen atmosphere.

2.4. Device fabrication

FTO glass substrates (Nippon Sheet Glass, Hyogo, Japan, TEC-14) were treated with mixing solution of hydrogen peroxide and ammonia and then were cleaned in solution of detergent, deionized water, acetone and ethanol, respectively. An isopropoxide solution (350 μL titanium(IV) isopropoxide (97%, Alfa Aesar) in 5 mL of ethanol with 0.013 M HCl) was spin coated onto precleaned FTO substrate at 2000 rpm for 30 s and sintering the resultant substrate at 500 °C for 30 min for obtaining a 30–50 nm dense blocking TiO_2 (bl-TiO_2) layer. Then, TiO_2 colloidal solution (20 nm TiO_2 : terpineol : ethanol = 1 : 1 : 3, weight ratio) was spin-coated onto bl-TiO_2 layer at 1500 rpm for 30 s. The resultant colloid-deposited FTO substrate was sintered at 500 °C for 30 min for attaining a mesoporous TiO_2 (mp-TiO_2) layer with the thickness of 300–400 nm. The film was immersed in 0.04 M aqueous $TiCl_4$ at 70 °C for 40 min. After cooling to

room temperature, the film was rinsed by deionized water and ethanol, respectively. Then the film was annealed at 500 °C for 30 min. The $CH_3NH_3PbI_3$ perovskite was obtained in two steps. Firstly, N,N-dimethylformamide (DMF, 99.8%, Aldrich) solution of 1.0 M PbI_2 (99%, Aldrich) were dropped onto the substrate of FTO/bl-TiO_2/mp-TiO_2 by spin-coating at 3000 rpm for 30 s, and then stirring the film at 70 °C for 15 min under N_2 protection. Secondly, the $CH_3NH_3PbI_3$ film was obtained by immerging the film in isopropanol (99.8%, Aldrich) of 0.06 M CH_3NH_3I and drying it on a hot plate at 100 °C for 15 min. After cooling down to room temperature, the HTM solution (3.5 mg in chlorobenzene of 1 mL) was spin-coating on top of the FTO/Bl-TiO_2/mp-TiO_2/$CH_3NH_3PbI_3$ substrate at 2000 rpm for 30 s. The carbon cathode prepared by graphite powder (20 nm, Chenyang Graphite, China) were deposited on the film and scraped to a fixed active area of 0.09 cm^2.

2.5. Photovoltaic characterizations

The photocurrent density voltage curves (J–V) characteristics of the PSC devices were carried out using a Keithley 2400 digital source meter controlled by a computer and a standard AM1.5 solar simulator-Oriel 91160-1000 (300 W) SOLAR SIMULATOR 2 × 2 BEAM. The light intensity was calibrated by an Oriel reference solar cell. To prevent inflated photocurrents arising from stray light, a 0.09 cm^2 black metal mask (cm^2) surrounded the active area was covered on a testing cell during all measurements. The action spectra of monochromatic incident photon-to-current conversion efficiency (IPCE) for solar cell were performed by using a commercial setup (QTest Station 2000 IPCE Measurement System, CROWNTECH, USA). Intensity modulated photovoltage spectroscopes (IMVS) was also measured by the Zennium electrochemical workstation (ZAHNER, Germany), in which a green light emitting diode (LED, 532 nm) was modulated to yield light frequency ranging from 100 mHz to 10 kHz and illumination intensity from 1 to 40 mW cm^{-2}. Electron densities were measured by charge extraction technique as reported.[51]

3. Results and discussion

3.1. Spectral characterizations

The light absorption property and optical energy gap (E_g^{opt}) of **Q197**, **Q198** and **Q205** were studied, and the spectra of the HTMs are shown in Fig. 2. The corresponding spectroscopic data are listed in Table 1. Fig. 2(a) shows the normalized UV-visible absorption and fluorescence emission spectra of the three HTMs in dichloromethane. The maximum absorption wavelength (λ_{abs}^{max}) of **Q197**, **Q198** and **Q205** are located at 389 nm, 389 nm and 307 nm, respectively. The absorption bands of **Q197** and **Q198** exhibited a red shift compared to **Q205**, and this may be due to the introduction of 4-methoxy-phenyl-amine substituted on 2,7-positions of 9H-carbazole extending the conjugation length of **Q197** and **Q198**. The molar extinction coefficient of **Q197**, **Q198** and **Q205** are 62 224 M^{-1} cm^{-1}, 51 966 M^{-1} cm^{-1}, and 109 075 M^{-1} cm^{-1}, respectively (Fig. 2(b)). Obviously, **Q205** and **Q197** exhibit higher molar
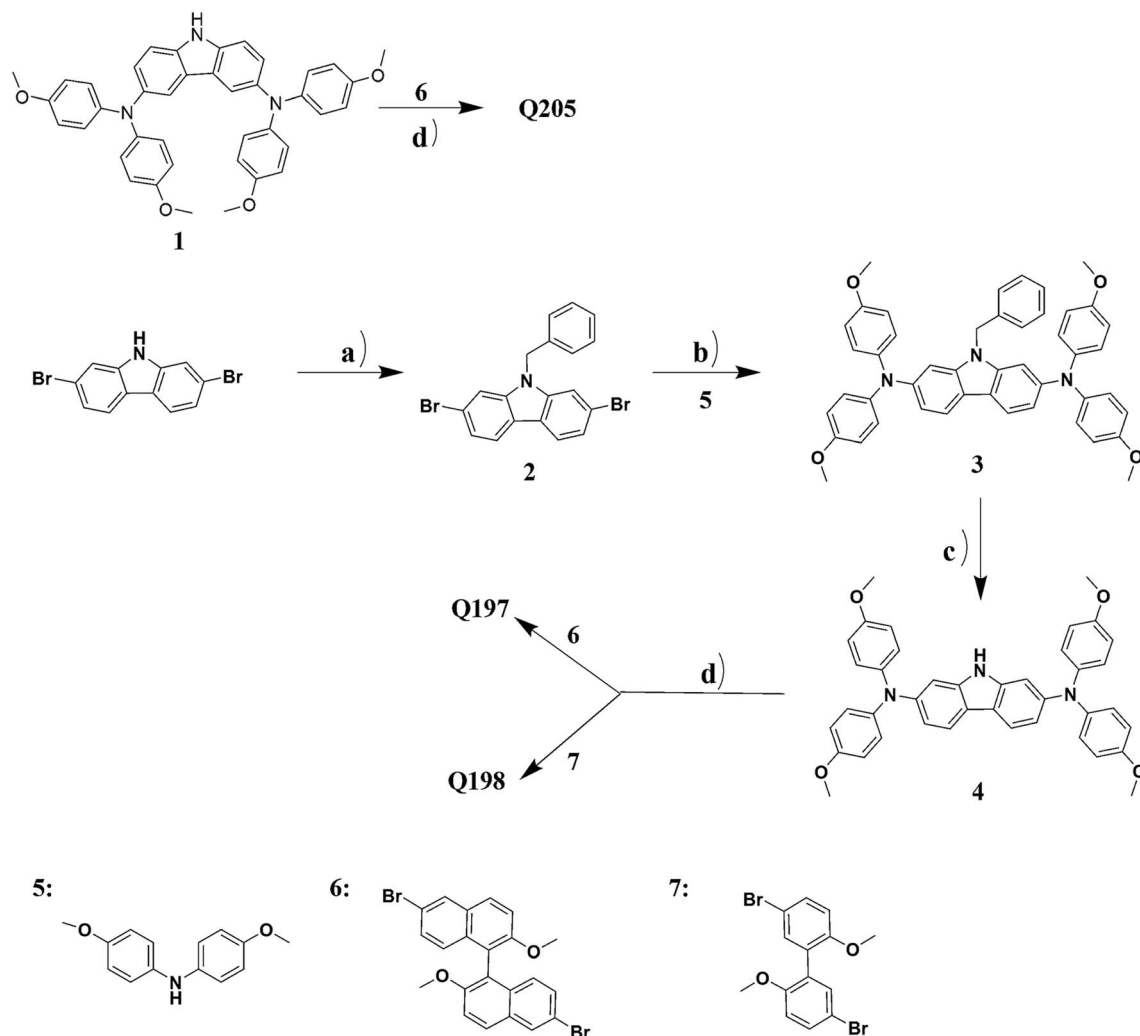
Scheme 1 The synthesis route of **Q205**, **Q197** and **Q198**. Conditions: (a) benzyl bromide, NaH, DMF, RT, 6 h, quantitative yield; (b) 4,4′-dimethoxydiphenylamine, Pd$_2$(bda)$_3$, (t-Bu)$_3$P, t-BuONa, toluene, reflux, overnight; (c) t-BuOK, DMSO, O$_2$, rt, overnight, (63%); (d) Pd$_2$(bda)$_3$, (t-Bu)$_3$P, t-BuONa, toluene, reflux, 24 h.

extinction coefficient than **Q198**. The maximum emission wavelength (λ_{fl}^{max}) of **Q205**, **Q197** and **Q198**, are 476 nm, 428 nm and 427 nm, and the corresponding optical band gaps (E_g^{opt}) calculated from the spectroscopic data are 2.60 eV, 2.90 eV and 2.90 eV,[28] respectively. Fig. 2(c) displays the absorption spectra of HTMs coated on TiO$_2$ (**Q205**/TiO$_2$, **Q197**/TiO$_2$ and **Q198**/TiO$_2$) and HTMs coated on perovskite (CH$_3$NH$_3$PbI$_3$)/TiO$_2$ films (**Q205**/CH$_3$NH$_3$PbI$_3$/TiO$_2$, **Q197**/CH$_3$NH$_3$PbI$_3$/TiO$_2$ and **Q198**/CH$_3$NH$_3$PbI$_3$/TiO$_2$). The **Q205**/TiO$_2$, **Q197**/TiO$_2$ and **Q198**/TiO$_2$ films mainly exhibit UV absorption. The **Q205**/CH$_3$NH$_3$PbI$_3$/TiO$_2$, **Q197**/CH$_3$NH$_3$PbI$_3$/TiO$_2$ and **Q198**/CH$_3$NH$_3$PbI$_3$/TiO$_2$ films display an enhancement of absorption in the visible range from 400 to 750 nm, comparing to CH$_3$NH$_3$PbI$_3$/TiO$_2$ film.

3.2. Quantum chemical calculations

The electronic properties and geometries of **Q205**, **Q197** and **Q198** were investigated by quantum chemical calculations. DFT at the B3LYP/6-31g level was used to optimize the geometric structures of the three HTMs. All structural optimization and energy calculations were performed using the GAUSSIAN 09 program. The optimized structures of **Q205**, **Q197** and **Q198** are shown in Fig. S1 (ESI†), and the atoms are numbered. The selected bond angles and bond lengths of **Q205**, **Q197** and **Q198** are presented in Table S1.† The length of C–N bond binding 9H-carbazole and (4-methoxy-phenyl)-amine on 3,6-substituted position of **Q205** is 1.430 Å, and that on 2,7-substituted position of **Q197** is shorter (1.426 Å). The representative dihedral angles of the three HTMs are marked, as shown in Fig. S2.† The two naphthalene rings of BINOL have a 3D structure with a dihedral angle of 75.427° in **Q205** and 99.341° in **Q197**. The frontier orbitals of molecules are also studied (Fig. 3). The highest occupied molecular orbital (HOMO) and the lowest unoccupied molecular orbital (LUMO) of three HTMs were simulated using Gaussian 09 program. The HOMO of **Q205**, **Q197** and **Q198** is localized in the carbazole–diarylamine part, and the LUMO mainly localized in the central core. It is indicated that a photoinduced electron transfer can occur in the HTM compounds by the HOMO–LUMO excitation.
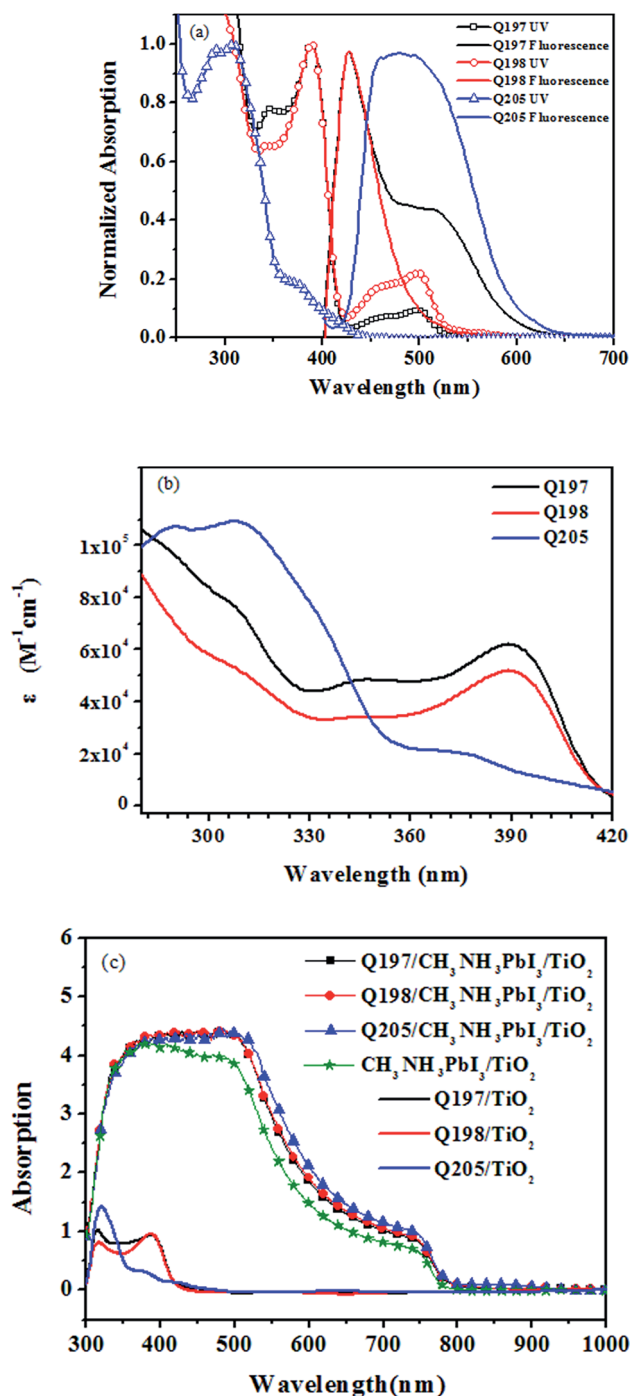
Fig. 2 (a) Normalized absorption and fluorescence emission spectra of **HTMs** in dichloromethane solution. (b) The corresponding molar extinction coefficient of absorption spectra in dichloromethane solution. (c) UV-vis spectra of **HTMs** on TiO$_2$ **HTMs** on perovskite (CH$_3$NH$_3$PbI$_3$)/TiO$_2$ and perovskite (CH$_3$NH$_3$PbI$_3$)/TiO$_2$ in thin films.

3.3. Electrochemical measurements

The accurate HOMO level of **Q205**, **Q197** and **Q198** were determined by cyclic voltammetry (CV), and the CV curves are shown in Fig. 4. Table 2 lists the corresponding electrochemical data of the three HTMs. The HOMO levels of **Q205**, **Q197** and **Q198** calculated from CV are −5.34 eV, −5.39 eV and −5.40 eV,

Table 1 The spectroscopic data of compound **Q205**, **Q197** and **Q198** employed in solution and in solid–state films

Compound	λ_{abs}^{max} (nm) soln	λ_{fl}^{max} (nm) soln	ε/M^{-1} cm^{-1}	λ_{abs}^{max} (nm) film
Q197	389	428	62 224	316
				387
Q198	389	427	51 966	316
				387
Q205	307	476	109 075	320

respectively.[52] The HOMO levels of the three HTMs are between that of CH$_3$NH$_3$PbI$_3$ (−5.43 eV) and the carbon counter electrode (−5.0 eV).[27,53–55] The LOMO levels of **Q205**, **Q197** and **Q198** are −2.38 eV, −2.36 eV and −2.37 eV, respectively. The LUMO value of HTMs higher than that of CH$_3$NH$_3$PbI$_3$ (−3.93 eV) favors electron injection efficiency on the surface of CH$_3$NH$_3$-PbI$_3$/HTM.[16]

3.4. Thermal properties

The thermal stability of the studied HTMs was tested by thermogravimetry (TG) and differential scanning calorimetry (DSC). The TG and DSC results were plotted in Fig. 5. The three HTMs exhibit high thermal decomposition temperature (T_d) above 420 °C (Fig. 5(a)). **Q205**, **Q197** and **Q198** have a high glass transition temperature (T_g) of 188 °C, 168 °C and 157 °C (Fig. 5(b)). The naphthyl on the BINOL core has a stronger rigidity than the phenyl on the 3,3′-biphenyl core, and the BINOL core has a more twisted dihedral angle than the 3,3′-biphenyl core (Fig. S2†). The much higher T_g values of **Q205** and **Q197** are possibly benefited from the more twisted structure of their BINOL central core than that of 3,3′-biphenyl core on the reference HTM (**Q198**).[56,57] In spin coating procedure, all of them can form amorphous films in solid states without molecular aggregation.

3.5. Device performance

The morphology of spin-coated thin films of **Q205**, **Q197** and **Q198** on perovskite surface was measured by SEM (Fig. 6). The CH$_3$NH$_3$PbI$_3$ were prepared by two-step deposition. As shown in Fig. 6(a)–(c), the HTM films are transparent and uniform, and the result is in agreement with their good thermal stability showing no aggregation. Fig. 6(d) gives the cross-section SEM morphology of PSC, and the film thickness of HTM is 150 nm.

The photovoltaic performances of PSCs fabricated by BINOL-based HTMs were investigated by J–V characteristics under illumination of 100 mW cm^{-2}, and PSCs based on the reference HTM were also tested. In PSC devices, carbon counter electrode was used to replace noble metallic materials. At first, the conditions of HTM concentration, doping amount of LiTFSI and TBP were optimized. The results are shown in Fig. S3 and S4,† and the corresponding photovoltaic parameters are listed in Tables S2–S4 (ESI†). As shown in Fig. S3(b) and Table S2,† the best performance of **Q197**-based PSC is obtained under conditions of **Q197** (70 mg mL^{-1}) doping Li-TFSI/TBP (30 mM/120
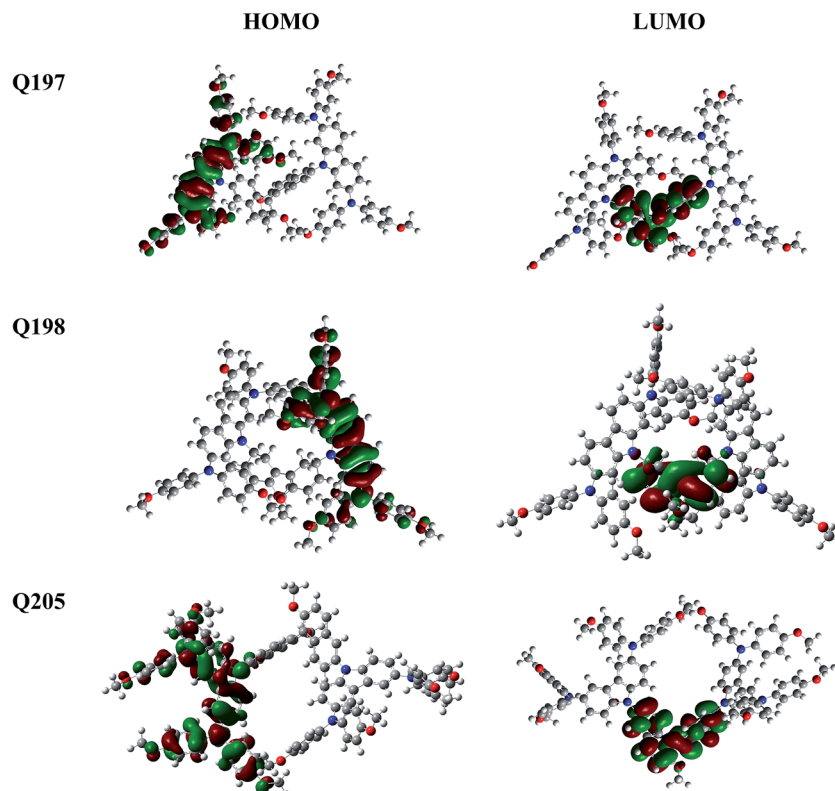
HOMO **LUMO**

Q197

Q198

Q205

Fig. 3   The frontier orbitals of **Q205**, **Q197** and **Q196**.

mM), leading to a short-circuit current density (J_{sc}) of 16.53 mW cm^{-2}, an open-circuit voltage (V_{oc}) of 897 mV, a fill factor (FF) of 0.56, and a PCE of 8.38%. This result is comparable to PSC based on commercial spiro-OMeTAD measured under the same condition (8.73%). At the same doping level, devices based on **Q205** and **Q198** got the PCE of 5.38% and 5.21%, respectively (Tables S2–S4†). When **Q197** of 30 mg mL^{-1} and 50 mg mL^{-1} was respectively used with addition of Li-TFSI/TBP (30 mM/120

mM), the corresponding PCE are 4.09% and 5.29%. When the concentration of **Q197** was increased from 70 mg mL^{-1} to 100 mg mL^{-1} (Li-TFSI/TBP (30 mM/120 mM)), the PCE decreased to 5.59%. Too higher concentration of HTM will form too thick solid-state film by spin coating, possibly resulting in the acceleration of electron recombination rate at the CH$_3$-NH$_3$PbI$_3$/HTM interface. PSC based on **Q197** without doping showed a J_{sc} of 11.14 mW cm^{-2}, a V_{oc} of 645 mV, a FF of 0.34, and a PCE of 2.45%. The doping of Li-TFSI and TBP has a positive impact on the photovoltaic action of HTM in PSC. As mentioned above, the optimal dosage of Li-TFSI and TBP for **Q197** are 30 mM and 120 mM, respectively. When the adding amount of Li-TFSI was kept at 30 mM, the PCE of PSC based on **Q197** doping TBP of 60 mM and 200 mM are 6.37% and 8.08%, respectively. In addition, when the adding amount of TBP was kept constant, the PCE of PSC based on **Q197** doping Li-TFSI of 60 mM and 15 mM are 3.91% and 4.18%, respectively. The positions of the end groups also have a great impact on the cell performance. In this work, the solubility of **Q197** and **Q198** based on 2,7-carbazole-bis(4-methoxy-phenyl)-amine in
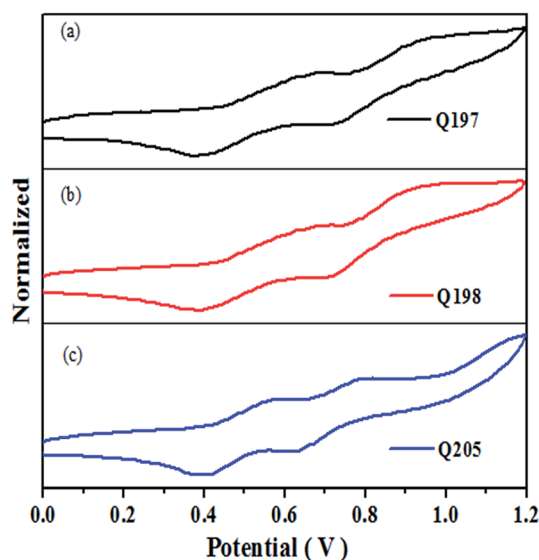

Fig. 4   Cyclic voltagrams of **Q205**, **Q197** and **Q198**.

Table 2   The electrochemical data of **Q205**, **Q197** and **Q198**

Compound	E_{pc} (V)	E_{pa} (V)	$E_{ox,1/2}$ (V)	E_{HOMO} (eV)	E_{LUMO} (eV)
Q205	0.40	0.56	0.54	−5.34	−2.38
Q197	0.39	0.67	0.59	−5.39	−2.36
Q198	0.39	0.69	0.60	−5.40	−2.37
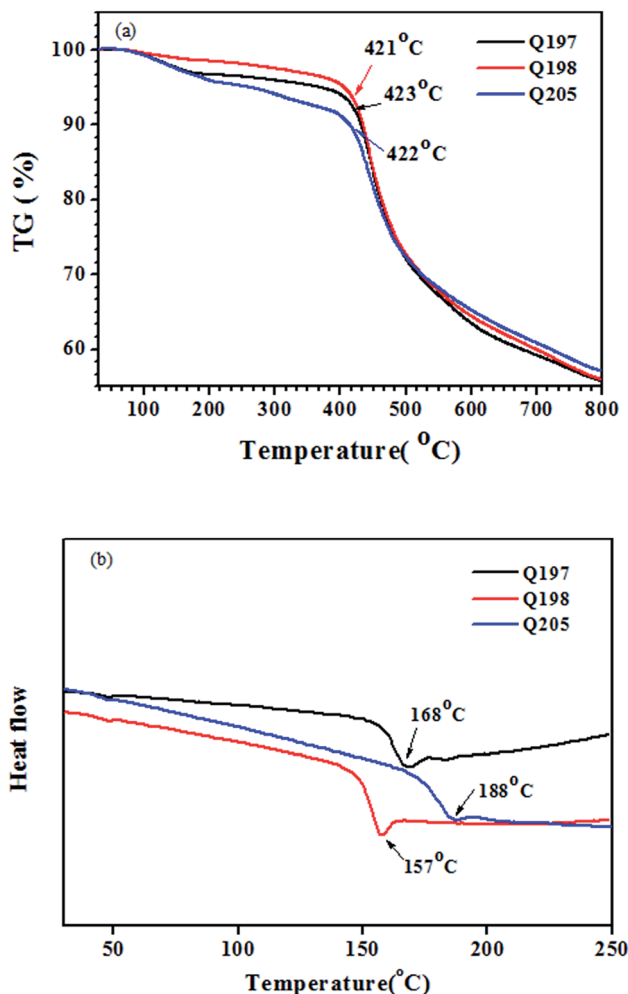
Fig. 5 (a) TG and (b) DSC curves of **Q205**, **Q197** and **Q198**.
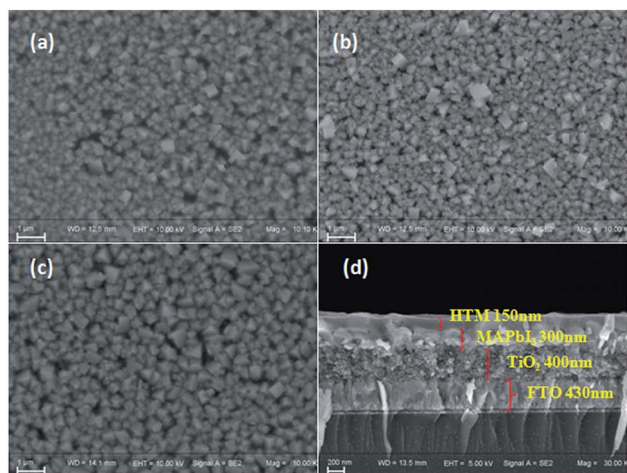

Fig. 6 Top SEM pictures of (a) **Q197**; (b) **Q198**; (c) **Q205**, and (d) cross-section SEM of PSC.

chlorobenzene is superior to that of **Q205** based on 3,6-carbazole-bis(4-methoxy-phenyl)-amine. The solubility of **Q205** was greatly enhanced when doping Li-TFSI/TBP of 30 mM/

200 mM. As shown in Fig. S3(a) and Table S3,† the optimized **Q205**-based PSC is fabricated under the condition of **Q205** (60 mg mL^{-1}) doping Li-TFSI/TBP (30 mM/200 mM), leading to a J_{sc} of 13.23 mW cm^{-2}, a V_{oc} of 984 mV, a FF of 0.50, and a PCE of 6.51%. As a comparison, the reference HTM **Q198**-based PSC showed the highest PCE of 7.08% under the condition of **Q198** (70 mg mL^{-1}) doping with Li-TFSI/TBP (30 mM/200 mM), yielding a J_{sc} of 16.69 mW cm^{-2}, a V_{oc} of 863 mV, a FF of 0.49. Therefore, the appropriate concentration of HTM concentration and doping amount of additives (Li-TFSI and TBP) improves the photovoltaic performances of PSC fabricated by BINOL-based HTM greatly.

Accordingly, J–V measurements of PSC based on HTMs **Q197/Q205/Q198** under illumination of 100 mW cm^{-2} and in dark were investigated. Fig. 7 shows the corresponding J–V characteristics of PSCs and the incident photon-to-current conversion efficiency (IPCE) spectra of devices.[58,59] The corresponding photovoltaic parameters are given in Table 3. From Fig. 7(a), PSC based on **Q197** (8.38%) exhibited better photovoltaic performance than that based on **Q205** (6.51%) and **Q198**
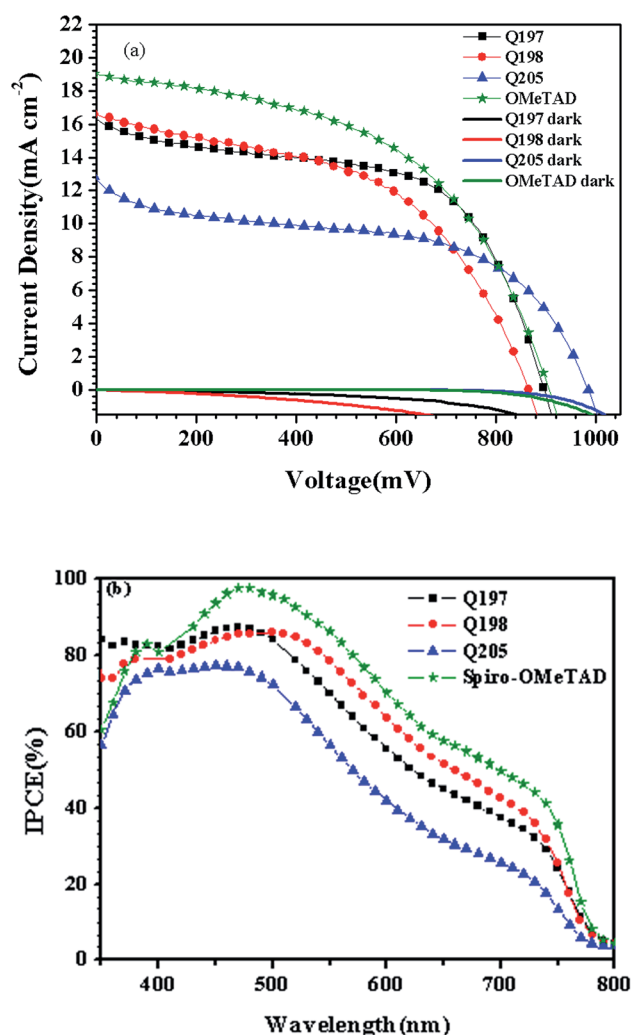

Fig. 7 (a) J–V and (b) IPCE characteristics of the optimal PSCs based on HTMs **Q197Q198Q205**\commerical spiro-OMeTAD.

(7.08%). The BINOL central core of **Q197** is superior to the 3,3′-biphenyl central core of **Q198**. The closer HOMO levels of **Q197** (-5.39 eV) and **Q198** (-5.40 eV) to the valence band of CH$_3$NH$_3$PbI$_3$ than **Q205** (-5.34 eV) may promote holes to transfer from CH$_3$NH$_3$PbI$_3$ to HTM layer. It is also shown in Fig. 7(a) that the dark current of PSC was increased in order of **Q205** < **Q197** < **Q198**. This result suggests that charge recombination of **Q205** and **Q197** was greatly reduced.[60] The higher V_{oc} value of **Q205** (984 mV) and **Q197** (897 mV) than **Q198** (863 mV) may caused by the decrease of charge recombination.[46] Thus, BINOL-based HTMs has a great potential for the construction of highly efficient PSCs. The J_{sc} of PSC increased in order of **Q205** (13.23 mW cm^{-2}) < **Q197** (16.53 mW cm^{-2}) ≈ **Q198** (16.69 mW cm^{-2}), which was in accordance with IPCE value (Fig. 7(b)).

To further evaluate the potential of the studied HTMs, time constant of electron recombination (τ_n) was measured by intensity modulated photovoltage spectroscopy (IMVS)[61] (Fig. 8). As shown in Fig. 8, PSC based on **Q197** and **Q198** show a lager time constant of electron recombination and a higher electron density than that based on **Q205**. This result is agreement with that **Q197** and **Q198** exhibited higher J_{sc} values than **Q205**. Based on the results of J–V characteristics, it can be concluded that the change of donor arms of BINOL-based HTMs can be used to regulate the photovoltaic parameters of

Table 3 J–V characteristics of optimal photovoltaic parameters of PSC

HTM	J_{sc}/mA cm^{-2}	V_{oc}/V	FF	$\eta\%$
Q197[a]	16.53	897	0.56	8.38
Q198[b]	16.69	863	0.49	7.08
Q205[c]	13.23	984	0.50	6.51
Spiro-OMeTAD[b]	18.98	906	0.51	8.73

[a] 70 mg mL^{-1} HTM doped with 30 mM Li-TFSi/120 mM TBP. [b] 70 mg mL^{-1} HTM doped with 30 mM Li-TFSi/200 mM TBP. [c] 60 mg mL^{-1} HTM doped with 30 mM Li-TFSi/200 mM TBP.
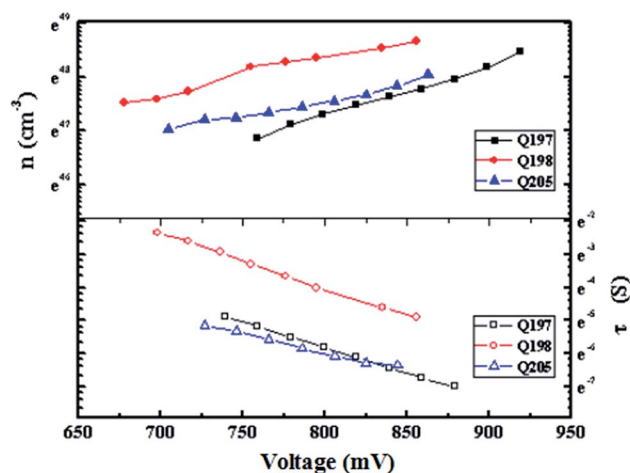

Fig. 8 Plots of the recombination time constant (τ_n) and electron density (n) versus open circuit voltage of PSCs based on HTMs **Q197Q198Q205**.

PSCs. **Q197** containing 2,7-carbazole-bis(4-methoxy-phenyl)-amine groups exhibits higher J_{sc}. **Q205** bearing 3,6-carbazole-bis(4-methoxy-phenyl)-amine shows lager V_{oc}. Moreover, Table S5† lists photovoltaic parameters of eight cells fabricated by **Q197**. It is shown that PSCs fabricated by BINOL-based HTMs displayed replicability, which is good for BINOL-based HTMs to become a promising candidate for the fabrication of efficient PSCs.

4. Conclusion

Two star-shaped HTMs based on a 1,1′-bi-2-naphthol (BINOL) central core for perovskite solar cells are synthesized by a facile route. BINOL is aimed to be used as a bridged/spiro core for preparing comparable HTM to commercial spiro-OMeTAD. The BINOL core is armed with end groups of 3,6-carbazole-bis(4-methoxy-phenyl)-amine (**Q205**) and 2,7-carbazole-bis(4-methoxy-phenyl)-amine (**Q197**), separately. A reference HTM based on a 3,3′-biphenyl core and 2,7-carbazole-bis(4-methoxy-phenyl)-amine was prepared for comparison (**Q198**). The optimized geometric structures display the two naphthalene rings of BINOL with a dihedral angle of 75.427° in **Q205** and 99.341° in **Q197**. The two phenyl rings of the 3,3′-biphenyl core on the reference HTM show a dihedral angle of 114.004°. Thus, BINOL-based HTMs with more twisted structures display much higher T_g values ($T_g > 160$ °C) than the reference HTM. CV data show **Q197** containing 2,7-carbazole-bis(4-methoxy-phenyl)-amine have deeper HOMO level than **Q205** containing 3,6-carbazole-bis(4-methoxy-phenyl)-amine, leading to closer energy gap to the valence band of CH$_3$NH$_3$PbI$_3$. J–V characteristics results show device based on **Q197** display a higher J_{sc} and the highest PCE (8.38%) than **Q205** (6.51%), which is comparable to that fabricated by commercial spiro-OMeTAD (8.73%). Device fabricated by **Q205** shows a much larger V_{oc} (983 mV). The dark current measurements indicate the BINOL-based HTMs effectively reduced charge recombination, as compared to the reference HTM. IMVS measurements also show BINOL-based HTMs have large time constant of electron recombination and high electron density. Therefore, BINOL is a promising bridge/spiro building block for fabricating highly efficient PSC, and the photovoltaic parameters of device based on this new type HTM can be flexibly tunable by structural modification.

Acknowledgements

References

1 D. Q. Bi, B. Xu, P. Gao, L. C. Sun, M. Grätzel and A. Hagfeldt, *Nano Energy*, 2016, **23**, 138.

2 T. Salim, S. Sun, Y. Abe, A. Krishna, A. C. Grimsdale and Y. M. Lam, *J. Mater. Chem. A*, 2015, **3**, 8943.

3 L. K. Ono, M. R. Leyden, S. H. Wang and Y. B. Qi, *J. Mater. Chem. A*, 2016, **4**, 6693.

4 M. Park, J. S. Park, K. Han and J. Young, *J. Mater. Chem. A*, 2016, **4**, 11307.

5 N. G. Park, *CrystEngComm*, 2016, **18**, 5977.

6 T. Salim, S. Y. Sun, Y. Abe, A. Krishna, A. C. Grimsdale and Y. M. Lam, *J. Mater. Chem. A*, 2015, **3**, 8943.

7 H. W. Chen, Y. Hou, C. E. Halbig, S. Chen, H. Zhang, N. Li, F. Guo, X. F. Tang, N. Gasparini, I. Levchuk, S. Kahmann, C. O. R. Quiroz, A. Osvet, S. Eigler and C. J. Brabec, *J. Mater. Chem. A*, 2016, **4**, 11604.

8 T. C. Sum and N. Mathews, *Energy Environ. Sci.*, 2014, **7**, 2518.

9 Y. X. Zhao and K. Zhu, *Chem. Soc. Rev.*, 2016, **45**, 655.

10 S. Q. Luo and W. A. Daoud, *J. Mater. Chem. A*, 2015, **3**, 8992.

11 U. Bach, D. Lupo, P. Comte, J. E. Moser, F. Weissortel, J. Salbeck, *et al.*, *Nature*, 1998, **395**, 583.

12 J. Liu, Y. Z. Wu, C. J. Qin, X. D. Yang, T. Yasuda, A. Islam, K. Zhang, W. Q. Peng, W. Chen and L. Y. Han, *Energy Environ. Sci.*, 2014, **7**, 2963.

13 S. Kazim, F. J. Ramos, P. Gao, M. K. Nazeeruddin, M. Grätzel and S. Ahmad, *Energy Environ. Sci.*, 2015, **8**, 1816.

14 G. F. Gong, N. Zhao, D. Ni, J. Y. Chen, Y. Shen, M. K. Wang and G. L. Tu, *J. Mater. Chem. A*, 2016, **4**, 3661.

15 Y. T. Shi, K. L. Hou, Y. X. Wang, K. Wang, H. C. Ren, M. Y. Pang, F. Chen and S. Zhang, *J. Mater. Chem. A*, 2016, **4**, 5415.

16 H. Nishimura, N. Ishida, A. Shimazaki, A. Wakamiya, A. Saeki, L. T. Scott and Y. Murata, *J. Am. Chem. Soc.*, 2015, **137**, 15656.

17 H. Choi, J. W. Cho, M. S. Kangc and J. Ko, *Chem. Commun.*, 2015, **51**, 9305.

18 M. L. Petrus, T. Bein, T. J. Dingemans and P. Docampo, *J. Mater. Chem. A*, 2015, **3**, 12159.

19 J. Wang, S. Wang, X. Li, L. Zhu, Q. Meng, Y. Xiao and D. Li, *Chem. Commun.*, 2014, **50**, 5829.

20 S. Lv, L. Han, J. Xiao, L. Zhu, J. Shi, H. Wei, Y. Xu, J. Dong, X. Xu, D. Li, S. Wang, Y. Luo, Q. Meng and X. Li, *Chem. Commun.*, 2014, **50**, 6931.

21 H. Choi, S. Park, S. Paek, P. Ekanayake, K. M. Nazeeruddinc and J. Ko, *J. Mater. Chem. A*, 2014, **2**, 19136.

22 B. Xu, E. Sheibani, P. Liu, J. B. Zhang, H. N. Tian, N. Vlachopoulos, G. Boschloo, L. Kloo, A. Hagfeldt and L. C. Sun, *Adv. Mater.*, 2014, **26**, 6629.

23 N. J. Jeon, J. Lee, J. H. Noh, M. K. Nazeeruddin, M. S. Grätzel and S. I. Seok, *J. Am. Chem. Soc.*, 2013, **135**, 19087.

24 K. Do, H. Choi, K. Lim, H. Jo, J. W. Cho, M. K. Nazeeruddinc and J. Ko, *Chem. Commun.*, 2014, **50**, 10971.

25 S. Y. Ma, H. Zhang, N. Zhao, Y. B. Cheng, M. K. Wang, Y. Shen and G. L. Tu, *J. Mater. Chem. A*, 2015, **3**, 12139.

26 T. Krishnamoorthy, F. Kunwu, P. P. Boix, H. R. Li, T. M. Koh, W. L. Leong, S. Powar, A. Grimsdale, M. Grätzel, N. Mathews and S. G. Mhaisalkar, *J. Mater. Chem. A*, 2014, **2**, 6305.

27 P. Ganesan, K. Fu, P. Gao, I. Raabe, K. Schenk, R. Scopelliti, J. S. Luo, L. H. Wong, M. Grätzel and M. K. Nazeeruddin, *Energy Environ. Sci.*, 2015, **8**, 1986.

28 S. M. Park, J. H. Heo, C. H. Cheon, H. Kim, S. H. Im and H. J. Son, *J. Mater. Chem. A*, 2015, **3**, 24215.

29 M. Maciejczyk, A. Ivaturi and N. Robertson, *J. Mater. Chem. A*, 2016, **4**, 4855.

30 T. Swetha and S. P. Singh, *J. Mater. Chem. A*, 2015, **3**, 18329.

31 B. Xu, D. Q. Bi, Y. Hua, P. Liu, M. Cheng, M. Grätzel, L. Kloo, A. Hagfeldt and L. C. Sun, *Energy Environ. Sci.*, 2016, **9**, 873.

32 J. Wang, Y. Chen, F. S. Li, X. P. Zong, J. L. Guo, Z. Sun and S. Xue, *Electrochim. Acta*, 2016, **210**, 673.

33 J. Wang, Y. Chen, M. Liang, G. Y. Ge, R. J. Zhou, Z. Sun and S. Xue, *Dyes Pigm.*, 2016, **125**, 399.

34 S. Tang, Z. Y. Wang, B. Liu and C. E. Dong, *Chin. Chem. Lett.*, 2015, **26**, 744.

35 R. H. Zheng, W. M. Wei, Y. Y. Jing, H. Liu and Q. Shi, *J. Phys. Chem. C*, 2013, **117**, 11117.

36 G. X. Du, Y. S. Li, S. N. Ma, R. Wang, B. Li, F. J. Guo, W. L. Zhu and Y. M. Li, *J. Nat. Prod.*, 2015, **78**, 2968.

37 G. W. Wang, A. X. Zhou, S. X. Li and S. D. Yang, *Org. Lett.*, 2014, **16**, 3118.

38 G. W. Wang, A. X. Zhou, S. X. Li and S. D. Yang, *Org. Lett.*, 2014, **16**, 3118.

39 M. N. Grayson and J. M. Goodman, *J. Am. Chem. Soc.*, 2013, **135**, 6142.

40 Q. S. Hu, D. Vitharana, X. F. Zheng, C. Wu, C. M. S. Kwan and L. Pu, *J. Org. Chem.*, 1996, **61**, 8370.

41 Y. Imai, K. Kamon, T. Kinuta, N. Tajima, T. Sato, R. Kuroda and Y. Matsubara, *Cryst. Growth Des.*, 2008, **8**, 3493.

42 Y. Imai, K. Kamon, T. Kinuta, N. Tajima, T. Sato, R. Kuroda and Y. Matsubara, *Cryst. Growth Des.*, 2009, **9**, 4096.

43 S. S. Yu, W. Plunkett, M. Kim, E. Wu, M. Sabat and L. Pu, *J. Org. Chem.*, 2013, **78**, 12671.

44 F. J. Miao, J. Zhou, D. M. Tian and H. B. Li, *Org. Lett.*, 2012, **14**, 3572.

45 S. S. Yu, A. M. DeBerardinis, M. Turlington and L. Pu, *J. Org. Chem.*, 2011, **76**, 2814.

46 X. P. Zong, Z. Sun, H. Wang, J. Wang, M. Liang and S. Xue, *Chem. Commun.*, 2015, **51**, 14076.

47 M. S. Kang, S. D. Sung, I. T. Choi, H. Kim, M. Hong, J. Kim, W. I. Lee and H. K. Kim, *ACS Appl. Mater. Interfaces*, 2015, **7**, 22213.

48 P. R. F. Barnes, K. Miettunen, X. Li, A. Y. Anderson, T. Bessho, M. Grätzel and B. C. O'Regan, *Adv. Mater.*, 2013, **25**, 1881.

49 H. Choi, S. Park and S. Paek, *J. Mater. Chem. A*, 2014, **2**, 19136.

50 Y. K. Song, S. T. Lv, X. C. Liu, X. G. Li, S. R. Wang, H. Y. Wei, D. Li, Y. Xiao and Q. Meng, *Chem. Commun.*, 2014, **50**, 15239.

51 G. D. Niu, W. Z. Li, F. Q. Meng, L. D. Wang, H. P. Dong and Y. Qiu, *J. Mater. Chem. A*, 2014, **2**, 705.

52 Z. S. Huang, H. L. Feng, X. F. Zang, Z. Iqbal, H. P. Zeng, D. B. Kuang, L. Y. Wang, H. Meierd and D. R. Cao, *J. Mater. Chem. A*, 2014, **2**, 15365.

53 H. S. Kim, C. R. Lee, J. H. Im, K. B. Lee, T. Moehl, A. Marchioro, S. J. Moon, R. Humphry-Baker, J. H. Yum, J. E. Moser, M. Grätzel and N. G. Park, *Sci. Rep.*, 2012, **2**, 00591.

54 F. G. Zhang, X. C. Yang, H. X. Wang, M. Cheng, J. H. Zhao and L. C. Sun, *ACS Appl. Mater. Interfaces*, 2014, **6**, 16140.

55 Z. L. Ku, Y. G. Rong, M. Xu, T. F. Liu and H. W. Han, *Sci. Rep.*, 2013, **3**, 3132.

56 H. Wang, A. D. Sheikh, Q. Y. Feng, F. Li, Y. Chen, W. L. Yu, E. Alarousu, C. Ma, M. A. Haque, D. Shi, Z. S. Wang, O. F. Mohammed, O. M. Bakr and T. Wu, *ACS Photonics*, 2015, **2**, 849.

57 S. Park, J. H. Heo, J. H. Yun, T. S. Jung, K. Kwak, M. J. Ko, C. H. Cheon, J. Y. Kim, S. H. Im and H. J. Son, *Chem. Sci.*, 2016, **7**, 5517.

58 J. Huang, M. Wang, L. Ding, J. Deng and X. Yao, *Semicond. Sci. Technol.*, 2016, **31**, 025009.

59 J. Huang, M. Wang, L. Ding, Z. Yang and K. Zhang, *RSC Adv.*, 2016, **6**, 55720.

60 N. Li, H. P. Dong, H. Dong, J. L. Li, W. Z. Li, G. D. Niu, X. D. Guo, Z. X. Wu and L. D. Wang, *J. Mater. Chem. A*, 2014, **2**, 14973.

61 G. D. Niu, W. Z. Li, F. Q. Meng, L. D. Wang, H. P. Dong and Y. Qiu, *J. Mater. Chem. A*, 2014, **2**, 705.